CHEMISTRY OF MATERIALS

Article

pubs.acs.org/cm

Microribbon Field-Effect Transistors Based on Dithieno[2,3-d;2,3′-d′]benzo[1,2-b;4,5-b′]dithiophene Processed by Solvent Vapor Diffusion

Suhao Wang,[†] Peng Gao,[†] Ingo Liebewirth,[†] Katrin Kirchhoff,[†] Shuping Pang,[†] Xinliang Feng,[†] Wojciech Pisula,*[,†,‡] and Klaus Müllen*[,†]

[†]Max Planck Institute for Polymer Research, Ackermannweg 10, 55128 Mainz, Germany

Supporting Information

ABSTRACT: Well-defined DTBDT crystal microribbons were fabricated by a solution processing method named as solvent vapor diffusion directly on the surface. This procedure is based on exposing a drop cast solution to a saturated solvent vapor atmosphere and allows to tune the dimensions of the ribbons simply by controlling the concentration of the solution. The structural study indicates single crystallinity and a molecular organization in the ribbons that is considered to be favorable for the carrier transport along ribbon axis. In the device, individual crystal DTBDT organic field-effect transistors exhibit mobilities as high as 3.2 cm^2 V^{-1} s^{-1} and on/off ratios up to 1×10^6. This processing approach can be further exploited for a broad range of other (macro)molecular semiconductors and additionally bears great potential for practical applications.

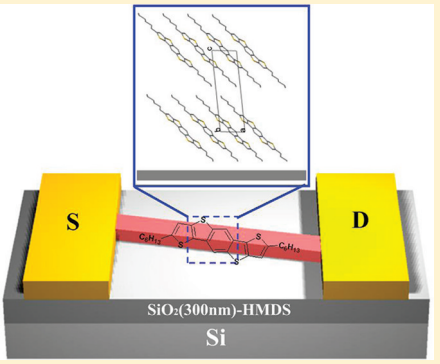

KEYWORDS: *microribbon, organic electronics, field-effect transistor, self-assembly, solution processing*

1. INTRODUCTION

Organic field-effect transistors (OFETs) based on one-dimensional (1D) nano- or microstructures have attracted continuous attention in recent years for their unprecedented device performance and thus hold great promise for the field of miniaturized organic and supramolecular electronics.[1] Among 1D nano- or microstructures, single-crystal mircoribbons or microwires are free of grain boundaries and molecular disorder, facilitating directional charge transport and excition diffusion.[2] High-performance OFETs based on such nano- and microsized single-crystal ribbons or wires have been reported for various small conjugated molecules. For instance, single-crystal OFETs based on copper phthalocyanine nanoribbon exhibited hole mobilities of 0.5 cm^2 V^{-1} s^{-1},[2a] whereas single-crystal microwires self-assembled from bis-phenylethyl-perylene-tetracarboxylic diimide showed an electron mobility of 1.4 cm^2 V^{-1} s^{-1}.[2b] Recently, mobilities even beyond 2.0 cm^2 V^{-1} s^{-1} were observed for n- as well as p-type OFETs based on single crystal ribbons of various small crystalline building blocks.[2c−f] Inspired by the high performance of the single-crystal ribbons, interest now is directed toward the assembly of the crystals and the study of their electronic properties.

Up to now, the most commonly used methods to fabricate organic single-crystals are vacuum deposition and drying the solution to recrystallize the molecules. These techniques yielded for various n- and p-type small molecules large two-dimensional single crystals with FET mobilities far above 3 cm^2 V^{-1} s^{-1}.[3] However, vacuum deposition is energy-consuming and requires the employment of equipment, whereas solution growth is time-consuming and takes the range of several hours up to few days. Recently, solution processing methods such as solvent vapor annealing (SVA)[2d,m] and precipitation in solvent mixtures[1a] have been successfully employed to induce 1D structures. Nevertheless, so far, it is still a challenge to grow organic single crystals directly on the substrate and to incorporate them into high performance FETs yielding mobilities above 1 cm^2 V^{-1} s^{-1}, which is desirable for the practical applications. In this communication, we report the utilization of solvent vapor diffusion (SVD),[4] which will be described in more detail later in this work, for the fabrication of micrometer-sized crystal ribbons of **1** (dithieno[2, 3-*d*;2′, 3′-*d*′]benzo[1,2-*b*;4,5-*b*′]dithiophene -DTBDT, Scheme 1). Interestingly, using cyclohexane as solvent for **1** and THF as solvent vapor for diffusion, more than hundred of micrometers long

Scheme 1. Molecular Structure of 1 (dithieno[2, 3-*d*;2′, 3′-*d*′]benzo[1,2-*b*;4,5-*b*′]dithiophene, DTBDT

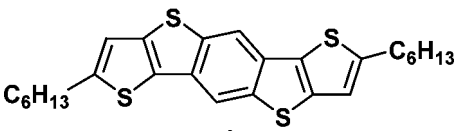

1

Received: July 20, 2011
Published: October 19, 2011

crystals are assembled only in several minutes, resulting in high p-type charge-carrier mobilities up to 3.2 $cm^2 V^{-1} s^{-1}$. The structural analysis indicates single crystallinity of these objects.

Thin film OFETs based on **1** exhibit hole mobilities of up to 0.01 $cm^2 V^{-1} s^{-1}$.[5a] Notably, this mobility is obtained on an untreated SiO_2 insulator surface and spin-coated films with only small crystalline domains, which hinder the charge transport due to numerous grain boundaries. This value was further increased to an average of 1.0 $cm^2 V^{-1} s^{-1}$ via dip-coating by extending the size of the crystalline domines.[5a] However, one can expect that this is not the ultimate device performance because inevitably, grain boundaries even in uniaxially oriented thin films affect the properties of semiconductors and reduce the charge carrier transport between the electrodes. On the basis of these data, it can be anticipated that higher hole mobilities could be achieved by further elevating the structural order of the molecules, for instance, in single-crystal ribbons.

2. EXPERIMENTAL SECTION

2.1. Self-Assembly via Solvent Vapor Diffusion. Several droplets of **1** solution in cyclohexane (around 20 μL) are drop cast on silicon wafer (1 × 1 cm^2) that is exposed to an airtight container saturated with solvent vapor (container volume: 500 mL filled with 50 mL of THF). Before the substrate was placed inside the container, a saturated solvent vapor atmosphere was created. It takes 5 min for the drop cast solution to evaporate completely in THF vapor. Here the evaporation rate can be tuned via changing the size of container without changing the THF amount. As soon as the drop fully evaporated, it was taken out of the container for characterization. For comparison, the same cyclohexane solution drop evaporates completely within 1.5 min in air. All experiments were performed under ambient temperatures.

2.2. Microribbon Characterizations. The micrographs of the ribbons were recorded using a Zeiss Axiophoto microscope (with and without polarizing filters) equipped with a Hitachi KP-D50 color digital CCD camera. AFM images were obtained with a Digital Instruments Nanoscope IIIa AFM in tapping mode. Transmission electron microscopy (TEM) was carried out on a FEI tecnai F30 ST at 300 kV under liquid N_2 cryoconditions. Electron diffraction pattern was recorded using a Philips CM 12 electron microscope at 120 V acceleration voltage. X-ray diffraction was performed on a θ–θ Philips PW 1820 Kristalloflex diffractometer with a graphite-monochromatized CuKα X-ray.

2.3. Device Fabrication and Measurements. For all devices, heavily doped silicon wafers with a thermally grown silicon dioxide layer 300 nm thick are used as substrates. The substrates were first cleaned using sonication in acetone for 10 min, following by sonication in isoproponal for 10 min, and finally these substrates were cleaned with oxygen plasma for 10 min. Following, a self-assembled monolayer of HMDS was deposited from the vapor phase using a vapor prime system at 135 °C for 60 min. For the bottom gate, top contact OFETs, source and drain electrodes with channel lengths of 25 μm are defined by a shadow mask, followed by Au evaporation to a height of 100 nm. All standard electrical measurements were performed in a glovebox under nitrogen atmosphere. For air-stability test, the transistors were measured in air. The device characteristics are measured with a Keithley 4200-SCS.

3. RESULTS AND DISCUSSION

To grow crystal microribbons on the surface, we systematically studied the self-assembly behavior of **1** via screening various solution processing methods. Simple drop casting of **1** from solution does not yield crystal objects or well-ordered thin films. Instead, inhomogeneous and disordered patches on the macroscopic scale appear when processed in this way from conventional solvents such as THF (Figure 2a), chloroform (Figure 2b), cyclohexane (Figure 2c), toluene, and chlorobenzene on HMDS-treated SiO_2 surface. Reducing the solvent evaporation rate by adding a cover over the droplet or by applying solvent vapor annealing on the dry thin layer does not distinctly change the film microstructure. As an additional processing method, the precipitation in solvent mixtures also does not result in surface crystals.

Therefore, SVD has been applied for the formation of crystal microribbons of **1**. This procedure is based on exposing a drop cast solution to a saturated solvent vapor atmosphere in an airtight container (Figure 1a). The first advantage of SVD is the fine adjustment of the evaporation rate of the solution by the right choice of the saturated solvent vapor. At the same time, polar/apolar cosolvent conditions can be established under which the solvent polarity forces solvophobic association between the alkyl side chains.[1a] Particularly, the large variety of processing parameters such as surface energy and solvent polarity in the solution and vapor opens the opportunity to fine balance dewetting effects and various forces including solvent-molecule, solvent–substrate, and molecule–substrate interactions in order to achieve the desired microstructure and molecular organization on the surface. It is important to underline that SVD significantly differs from SVA. As illustrated in Figure 1b, the later method is based on post treatment of a dry film in a saturated solvent vapor atmosphere.

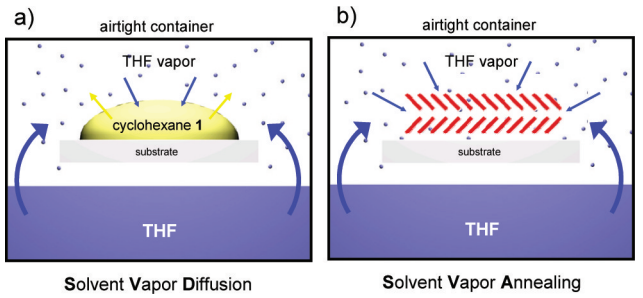

Figure 1. Schematic illustrations of (a) SVD and (b) SVA. During SVD, THF evaporates and saturates the atmosphere in an airtight container to which a drop of **1** cyclohexane solution is exposed. In contrast, during SVA, a dry film is treated by the saturated THF vapor.

After optimization of the SVD parameters such as solvent, concentration, vapor atmosphere, crystal microribbons on HMDS-treated SiO_2 silicon wafer were obtained in short time (5 min) by using cyclohexane as solvent for **1** solution at a concentration of 0.1–1.0 mg/mL and THF as solvent vapor. Thereby, THF vapor penetrates the cyclohexane solution and interacts with both **1** and cyclohexane (Figure 1b). This reduces the evaporation rate of the drop cast solution and provides polar/apolar cosolvent conditions under which the increase in solvent polarity forces solvophobic association between the alkyl side chains in a similar manner like during 1D self-assembly of surfactants and other amphiphilic molecules.[1i] As a great advantage of this method, the length of the microribbons is well-controlled from few tens to several hundred of micrometers by simply tuning the concentration of the compound in cyclohexane. At 0.1 mg/mL an average microribbon length of around ca. 20 μm is apparent (Figure 2d), whereas at 1.0 mg/mL, microribbons longer than 200 μm are grown (Figure 2f). The ribbon thickness also increases for higher concentration, but not in the same extent as the length (see Figure S1 in the Supporting Information). The thickness

dx.doi.org/10.1021/cm202844g | Chem. Mater. 2011, 23, 4960–4964

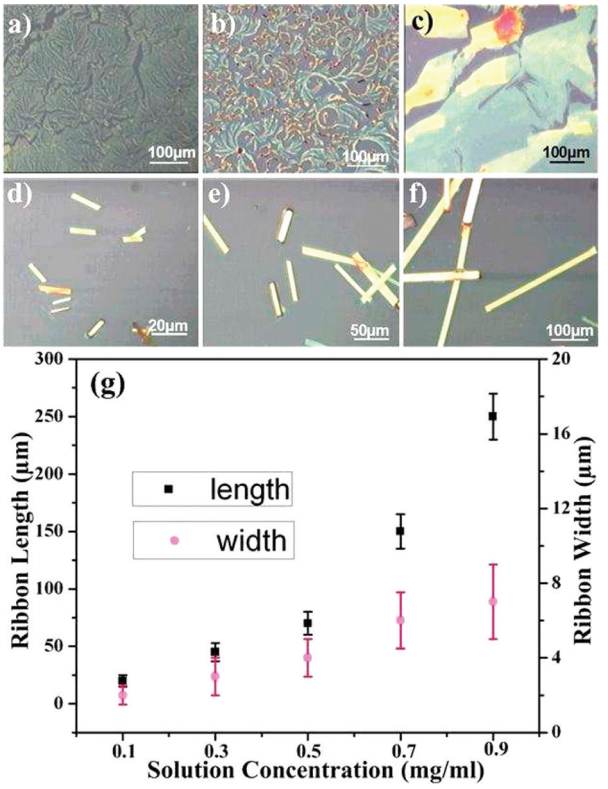

Figure 2. Reflection optical microscopy (OM) images of drop cast **1** from (a) THF, (b) chloroform, (c) cyclohexane on HMDS-treated silicon wafer; OM images of SVD **1** from cyclohexane under THF vapor at a concentration of (d) 0.1, (e) 0.5, and (f) 1.0 mg/mL, and (g) ribbon dimensions as a function of the solution concentration.

expands from an average value of 27 nm for 0.2 mg/mL to 68 nm for 1.0 mg/mL. Additionally, the variation in the thickness enlarges with increasing concentration. It has to be noted that the plot in Figure 2g does not take into account the number of formed ribbons for each concentration, but only displays the relation between dimensions of single ribbons and the concentration.

Under the cross-polarized optical microscope, the microribbons exhibit a pronounced homogeneous birefringence and strong optical anisotropy indicating high molecular order and uniform orientation within the ribbon. (Figure 3a) A typical microribbon scanned by an atomic force microscope (AFM) reveals also a uniform width of ca. 2 μm and height of 30 nm with an extremely low top surface roughness, which is an ideal candidate for FET applications (Figure 3c, 3d).

To elucidate the molecular structure of the crystal ribbons, a surface X-ray diffraction (XRD) in reflection mode was first performed for a macrosopically large area with randomly deposited ribbons (Figure 4a). Interestingly, although numerous ribbons scatter the X-ray at the same time, only peaks corresponding to a spacing of 1.85 nm appear. An identical diffractogram has been obtained for the dip-coated thin film of **1** indicating the same molecular arrangement on the surface.[5] For the ribbons, the spacing is close to the unit-cell parameter *c* of the single crystal[5a] and is oriented perpendicular to the surface. To further evaluate the exact arrangement of the two other crystal planes *a* and *b* within the ribbons, which are oriented parallel to the surface plane, transmission electron microscopy (TEM) was used. The corresponding image of the crystal microribbions is shown in Figure 4b confirming once

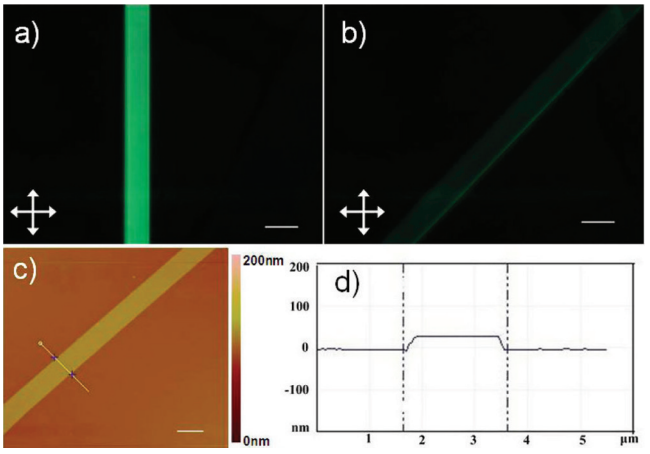

Figure 3. Cross-polarized optical images of microribbons obtained by SVD from **1** at (a) 0 and (b) 45° rotation toward the polarizers (scale in both POM images corresponds to 10 μm), (c) AFM image of a microribbon crystal (scale corresponds to 2 μm), and (d) height profile. The width and the height of the crystal are ca. 2 μm and 30 nm, respectively.

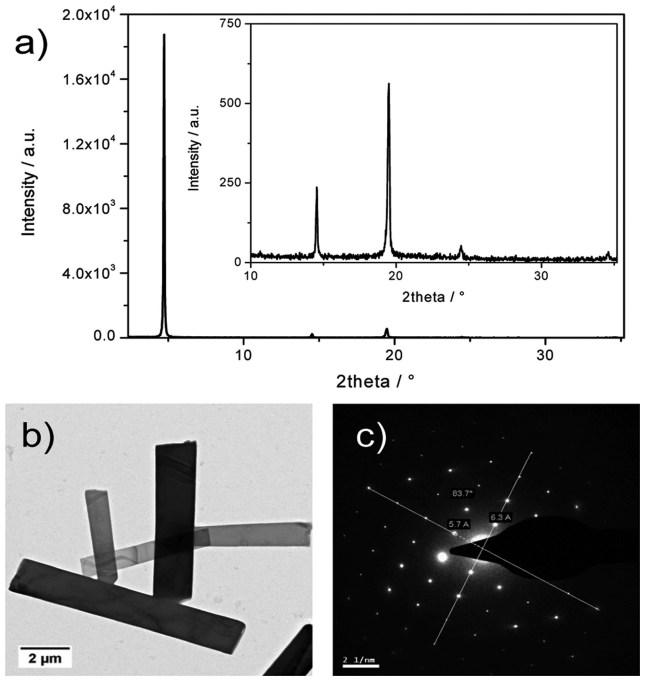

Figure 4. Structural investigation of the microribbons of **1** by (a) XRD, (b) TEM image, and (c) SAED pattern of one single ribbon.

again their regular rectangular shape. The deeper insight into the molecular organization is obtained from selected-area-diffraction (SAED) pattern for one ribbon (Figure 4c). No change in the SAED pattern is observed for different parts of the same ribbon, indicating single crystallinity of the 1D object. The analysis of the pattern revealed almost the same a = 0.57 nm and b = 0.63 nm unit parameters as found in the single crystal reported previously,[5a] whereby *a* and *c* are slightly larger in the ribbon. This minor increase can be related to the different processing SVD method yielding the ribbons. The crystal arrangement, in which the *a* plane is oriented along the ribbon axis, is illustrated in Figure 5a and is favorable for the transistor applications because it coincidences with the stacking direction and the charge carrier transport.[2d,6]

dx.doi.org/10.1021/cm202844g | *Chem. Mater.* 2011, 23, 4960–4964

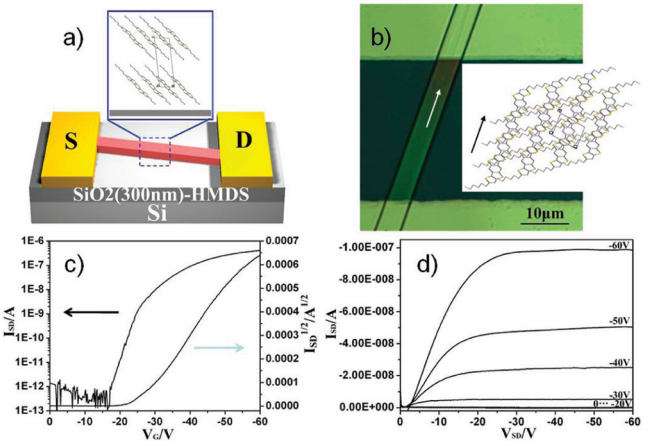

Figure 5. (a) Schematic illustration of the molecular arrangement in the ribbon OFET of **1**, (b) optical microscopy image of the individual ribbon OFET (white arrow indicates the crystal *a* axis) and the crystal structure in top view within the microribbon (black arrow indicates the ribbon axis), and corresponding (c) transfer and (d) output FET curves.

For few organic semiconductors a trend has been found between the crystal thickness and the charge carrier mobility in a transistor.[2d] In general, the mobility slightly increases with decreasing thickness, whereby it rises sharply below a critical thickness.[2o] For instance, the critical value is around 100 nm for F16CuPc and around 300 nm for pentacene. Therefore, crystal microribbons of **1** were processed at a concentration of 0.3 mg/mL for the FET applications yielding a length of 45 ± 8 μm, width of 4 ± 2 μm, and thickness of 40 ± 5 nm. The resulting microribbons were contacted using a shadow mask under an optical microscopy and OFETs were fabricated by evaporating source and drain gold electrodes, in this way establishing a bottom-gate, top-contact geometry (Figure 5a, 5b). All transistors exhibited typical *p*-channel field-effect characteristics. An average mobility of 1.8 ± 0.3 $cm^2 V^{-1} s^{-1}$, and an average on/off ratio of (6 ± 2) × 10^6 are determined for 20 individual devices, with the highest mobility of 3.2 $cm^2 V^{-1} s^{-1}$ achieved and an on/off ratio up to 6 × 10^6 (Figure 5c,d). Both the average and the highest mobility values represent approximately 2-fold improvement in comparison to the dip-coated film which is attributed to the increased molecular order and apparent reduction of domain boundaries within the transistor channel. Moreover, lower threshold voltages of −24 ± 5 V are obtained in comparison to the dip coated film (−39 ± 6 V) because of decreased charge trapping at the organic/insulator interface and within the semiconductor layer itself.[7] Although in this study an HMDS-treated SiO_2 dielectric monolayer has been employed to decrease the charge trapping at the organic/insulator interface, in our previous work, the dip-coated films were deposited on a untreated SiO_2 dielectric leading consequently to higher threshold voltages.[5a]

4. CONCLUSIONS

In conclusion, by a facile solution processing method named as solvent vapor diffusion, we successfully fabricated hundreds of micrometers long DTBDT crystal microribbons directly on SiO_2 surface within short time (5 min). The dimensions of the ribbons are tunable simply by controlling the concentration of the solution. The structural study indicates single crystallinity and a molecular organization in the ribbons which is considered to be favorable for the carrier transport along ribbon axis. In the device, individual crystal DTBDT OFETs exhibit mobilities as high as 3.2 $cm^2 V^{-1} s^{-1}$ and on/off ratio up to 1 × 10^6. It has to be emphasized that few examples of 2D single crystals lead to significantly higher mobilities, but their processing and device implementation is more demanding.[3] We believe that our processing approach can be further exploited for a broad range of other (macro)molecular semiconductors and additionally bears great potential for practical applications. The future challenge is the implementation of such high-performance ribbons in multiarray devices by using surface patterning to accurately place and align the objects toward the contacts.[8]

■ ASSOCIATED CONTENT

Ⓢ Supporting Information

Ribbon thickness as a function of concentration. This material is available free of charge via the Internet at http://pubs.acs.org.

■ AUTHOR INFORMATION

Corresponding Author

*E-mail: pisula@mpip-mainz.mpg.de; muellen@mpip-mainz.mpg.de.

Present Address

‡Evonik Industries AG, Kirschenallee, 64293 Darmstadt, Germany

■ ACKNOWLEDGMENTS

The German Science Foundation (Korean-German IR TG), the European Community's Seventh Framework Programme ONE-P (grant agreement n° 212311), DFG Priority Program SPP 1355, DFG MU 334/32-1, DFG Priority Program SPP 1459, and ESF Project GOSPEL (ref Nr: 09-EuroGRAPHENE-FP-001).

■ REFERENCES

(1) (a) Balakrishnan, K.; Datar, A.; Zhang, W.; Yang, X.; Naddo, T.; Huang, J.; Zuo, J.; Yen, M.; Moore, J. S.; Zang, L. *J. Am. Chem. Soc.* **2006**, *128*, 6576−6577. (b) Xiao, S.; Tang, J.; Beetz, T.; Guo, X.; Tremblay, N.; Siegrist, T.; Zhu, Y.; Steigerwald, M.; Nuckolls, C. *J. Am. Chem. Soc.* **2006**, *128*, 10700−10701. (c) Briseno, A. L.; Mannsfeld, S. C. B.; Lu, X.; Xiong, Y.; Jenekhe, S. A.; Bao, Z.; Xia, Y. *Nano Lett.* **2007**, *7*, 668−675. (d) Berson, S.; Bettignies, R. D.; Bailly, S.; Guillerez, S. *Adv. Funct. Mater.* **2007**, *17*, 1377−1384. (e) Samitsu, S.; Shimomura, T.; Heike, S.; Hashizume, T.; Ito, K. *Macromolecules* **2010**, *43*, 7891−7894. (f) Mu, X.; Song, W.; Zhang, Y.; Ye, K.; Zhang, H.; Wang, Y. *Adv. Mater.* **2010**, *22*, 4905−4909. (g) Lim, J. A.; Kim, J. H.; Qiu, L.; Lee, W. H.; Lee, H. S.; Kwak, D.; Cho, K. *Adv. Funct. Mater.* **2010**, *20*, 3292−3297. (h) Kim, F. S.; Ren, G.; Jenekhe, S. A. *Chem. Mater.* **2011**, *23*, 683−732. (i) Che, Y.; Datar, A.; Balakrishnan, K.; Zang, L. *J. Am. Chem. Soc.* **2007**, *129*, 7234−7235.

(2) (a) Tang, Q.; Li, H.; Song, Y.; Xu, W.; Hu, W.; Jiang, L.; Liu, Y.; Wang, X.; Zhu, D. *Adv. Mater.* **2006**, *18*, 3010−3014. (b) Oh, J. H.; Lee, H. W.; Mannsfeld, S.; Stoltenberg, R. M.; Jung, E.; Jin, Y. W.; Kim, J. M.; Yoo, J.; Bao, Z. *Proc. Natl. Acad. Sci.* **2009**, *106*, 6065−6070. (c) Zhou, Y.; Lei, T.; Wang, L.; Pei, J.; Cao, Y.; Wang, J. *Adv. Mater.* **2010**, *22*, 1484−1487. (d) Liu, C.; Minari, T.; Lu, X.; Kumatani, A.; Takimiya, K.; Tsukagoshi, K. *Adv. Mater.* **2011**, *23*, 523−526. (e) Jiang, W.; Zhou, Y.; Geng, H.; Jiang, S.; Yan, S.; Hu, W.; Wang, Z.; Shuai, Z.; Pei, J. *J. Am. Chem. Soc.* **2011**, *133*, 1−3. (f) Islam, Md. M.; Pola, S.; Tao, Y. T. *Chem. Commun.* **2011**, *47*, 6356−6358. (g) Zhou, Y.; Wang, L.; Wang, J.; Pei, J.; Cao, Y. *Adv. Mater.* **2008**, *20*, 3745−3749. (h) Liu, J.; Arif, M.; Zou, J.; Khondaker, S. I.; Zhai, L. *Macromolecules* **2009**, *42*, 9390−9393. (i) Li, R.; Hu, W.; Liu, Y.; Zhu, D. *Acc. Chem. Res.* **2010**, *43*, 529−540. (j) Jiang, L.; Dong, H.; Hu, W. *J. Mater. Chem.* **2010**, *20*, 4994−5007. (k) Li, R.; Dong, H.; Zhan, X.;

He, Y.; Li, H.; Hu, W. *J. Mater. Chem.* **2010**, *20*, 6014−6018. (l) Tang, Q.; Li, H.; He, M.; Hu, W.; Liu, C.; Chen, K.; Wang, C.; Liu, Y.; Zhu, D. *Adv. Mater.* **2006**, *18*, 65−68. (m) Mascaro, D. J.; Tompson, M. E.; Simth, H. I.; Bulovic, V. *Org. Electronics* **2005**, *6*, 211−220. (n) Dickey, K. C.; Anthony, J. E.; Loo, Y. *Adv. Mater.* **2006**, *18*, 1721−1726. (o) Jiang, H.; Tan, K. J.; Zhang, K. K.; Chen, X.; Kloc, C. *J. Mater. Chem.* **2011**, *21*, 4771−4773.

(3) (a) Jurchescu, O. D.; Baas, J.; Palstra, T. T. M. *Appl. Phys. Lett.* **2004**, *84*, 3061−3063. (b) Takahashi, Y.; Hasegawa, T.; Horiuchi, S.; Kumai, R.; Tokura, Y.; Saito, G. *Chem. Mater.* **2007**, *19*, 6382−6384. (c) Singh, Th. B.; Sariciftci, N. S.; Yang, H.; Yang, L.; Plochberger, B.; Sitter, H. *Appl. Phys. Lett.* **2007**, *90*, 213512−213512−3. (d) Takeya, J.; Yamagishi, M.; Tominari, Y.; Hirahara, R.; Nishikawa, Y.; Kawase, T.; Shimoda, T.; Ogawa, S. *Appl. Phys. Lett.* **2007**, *90*, 102120−102120−3. (e) Leufgen, M.; Rost, O.; Gould, C.; Schmidt, G.; Geurts, J.; Molenkamp, L. W.; Oxtoby, N. S.; Mas-Torrent, M.; Crivillers, N.; Veciana, J.; Rovira, C. *Org. Electronics* **2008**, *9*, 1101−1106. (f) Shukla, D.; Nelson, S. F.; Freeman, D. C.; Rajeswaran, M.; Ahearn, W. G.; Meyer, D. M.; Carey, J. T. *Chem. Mater.* **2008**, *20*, 7486−7491. (g) Jurchescu, O. D.; Subramanian, S.; Kline, R. J.; Hudson, S. D.; Anthony, J. E.; Jackson, T. N.; Gundlach, D. J. *Chem. Mater.* **2008**, *20*, 6733−6737. (h) Jiang, L.; Hu, W.; Wei, Z.; Xu, W.; Meng, H. *Adv. Mater.* **2009**, *21*, 3649−3653. (i) Molinari, A. S.; Alves, H.; Chen, Z.; Facchetti, A.; Morpurgo, A. F. *J. Am. Chem. Soc.* **2009**, *131*, 2462−2463.

(4) Wang, S.; Dössel, L.; Mavrinskiy, A.; Gao, P.; Feng, X.; Pisula, W.; Müllen, K. *Small* **2011**, *7*, 2841−2846.

(5) (a) Gao, P.; Beckmann, D.; Tsao, H. N.; Feng, X.; Enkelmann, V.; Baumgarten, M.; Pisula, W.; Müllen, K. *Adv. Mater.* **2009**, *21*, 213−216. (b) Li, L.; Gao, P.; Schuermann, K. C.; Ostendorp, S.; Wang, W.; Du, C.; Lei, Y.; Fuchs, H.; Cola, L. D.; Müllen, K.; Chi, L. *J. Am. Chem. Soc.* **2010**, *132*, 8807−8809.

(6) Izawa, T.; Miyazaki, E.; Takimiya, K. *Adv. Mater.* **2008**, *20*, 3388−3392.

(7) Scheinert, S.; Paasch, G.; Schrödner, M.; Roth, H.-K.; Sensfuß, S.; Doll, T. *J. Appl. Phys.* **2002**, *92*, 330−337.

(8) (a) Xu, Y.; Zhang, F.; Feng, X. *Small* **2011**, *10*, 1338−1360. (b) Mannsfeld, S. C. B.; Sharei, A.; Liu, S.; Roberts, M. E.; McCulloch, I.; Heeney, M.; Bao, Z. *Adv. Mater.* **2008**, *20*, 4044−4048.